

Geometrical sensitivity analysis based on design optimization and multiphysics analysis of PM assisted synchronous reluctance motor

V.S. NAGARAJAN^{1*}, V. KAMARAJ¹, and S. SIVARAMAKRISHNAN¹

Electrical and Electronics Engineering, SSN College of Engineering, Old Mahabalipuram Road, Kalavakkam, Tamil Nadu 603110, India

Abstract. Anisotropic rotor configurations influenced by the presence of a large number of geometrical parameters in a permanent magnet assisted synchronous reluctance (PMASR) motor pose design challenges in obtaining a robust geometry satisfying the requirements of reduced torque ripple and high torque density. Therefore, the purpose of this work is to perform detailed geometrical sensitivity analysis of a 36 slot/4 pole permanent magnet assisted synchronous reluctance (PMASR) motor using h-indexing and level sensitivity analysis in order to specify a guideline for designers to prioritize the design variables for optimization. Systematic multi-level design optimization for multiple objectives is implemented by an NSGA-II algorithm aided by the finite element analysis tool, hardware prototyping and experimental validation. The optimized designs also exhibit better structural and thermal characteristics.

Key words: PMASR motor, sensitivity analysis, finite element analysis (FEA), thermal analysis, stress analysis.

1. Introduction

Permanent magnet assisted synchronous reluctance [1–3] (PMASR) motor drives have established themselves as a unique and significant technology in recent times. They stand out particularly when compared with conventional motor drives, due to increased efficiency, improved torque density and reduction in volt ampere requirement, which results in turn from the presence of minimum quantities of ferrite magnets in a structured arrangement in the flux barriers.

Yet anisotropic rotor configurations influenced by the presence of a large number of geometrical parameters [4–8] in the PMASR motor rotor pose design challenges in obtaining a robust geometry satisfying the requirements of different applications. Therefore, it is necessary to perform design optimization [9–12], considering multiple objectives to enhance the motor's performance.

As the choice of the design variables for optimization is an important aspect influencing the end result, it is necessary to perform detailed sensitivity analysis to study their influence on the machine's performance. This work utilizes the h-indexing technique [9] and level sensitivity method [10] to perform geometrical sensitivity analysis and prioritize the design variables for optimization with respect to the objectives.

The prioritized design variables are optimized using the non-dominated sorting genetic algorithm – II (NSGA-II) [13, 14]. Finite element analysis (FEA) [15, 16] is also used for performance prediction in the optimization routine [11]. The design solutions are analyzed in a multiphysics environment to assess and highlight the structural and thermal characteristics [17–21].

The organization of the paper is as follows. Section 2 deals with performance analysis of the PMASR motor. In section 3, sensitivity analysis of motors based on two approaches is performed and design variables are grouped into strongly and mildly sensitive categories. This is followed by Section 4, which deals with the multi-objective design optimization routine using the NSGA-II algorithm. Section 5 presents thermal and stress analysis of optimum design solutions while Section 6 provides the conclusion.

2. Performance analysis of PMASR motor

The PMASR motor used in performance analysis is shown in Fig. 1.

The PMASR motor prototype design is based on significant contributions available in the literature, contributing towards improved average torque and reduced torque ripple. The op-

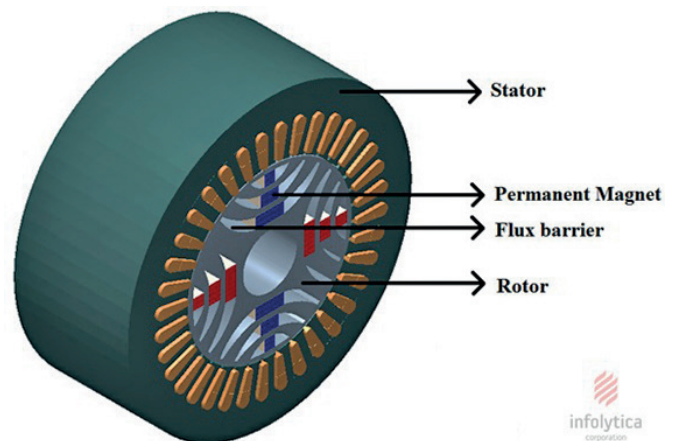


Fig. 1. 3D Model of PMASR motor

*e-mail: nagarajanvs@ssn.edu.in

Manuscript submitted 2017-12-29, revised 2018-03-12, initially accepted for publication 2018-03-19, published in February 2019.

timum slot/pole combination is decided to be 36/4 [4]. The number of flux barriers chosen is 3 [4–6]. The magnets are placed in increasing order of volume, from the rotor periphery to the shaft [6, 7]. The shape of flux barriers is similar to the shape used in [8, 9]. The angular positions at air gap are chosen from [8]. The CAD diagram defining the geometrical design parameters of one half cross section of the PMASR motor is presented in Fig. 2.

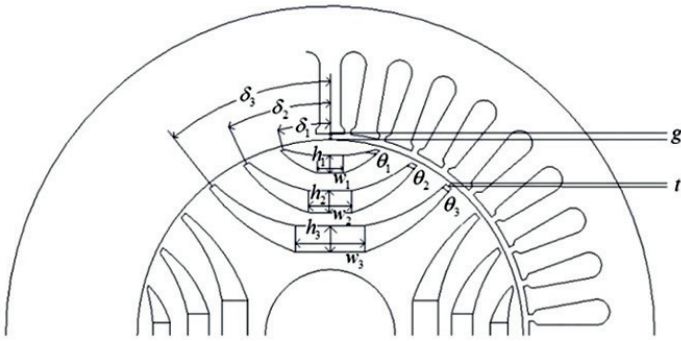


Fig. 2. Parametric model of a PMASR motor section

The rotor lamination and prototype of the PMASR motor used in the experiments for FEA validation are shown in Fig. 3 and Fig. 4, respectively. The specifications of the PMASR motor prototype are represented in Table A1 in the appendix to this text.



Fig. 3. Rotor lamination of PMASR motor

The performance characteristics of a PMASR motor are predicted using the finite element analysis (FEA) software [11, 22], MagNet 7.6.1 and MotorSolve 5.1. The magnetic flux density distribution at the rated operating conditions is presented in Fig. 5.

The experimental setup [7, 23] to validate the FEA model is shown in Fig. 6. The test setup consists of a fabricated prototype motor, controller, generator load, torque sensor and a PC for torque measurement display.



Fig. 4. PMASR motor rotor

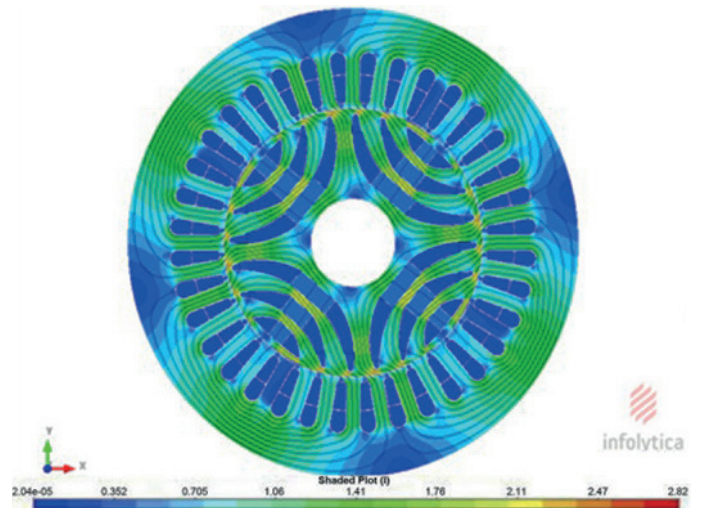


Fig. 5 Magnetic flux density distribution of a PMASR motor at rated operating conditions

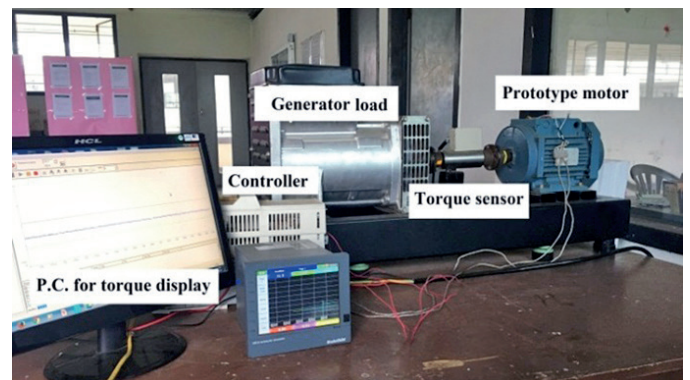


Fig. 6. Experimental test setup

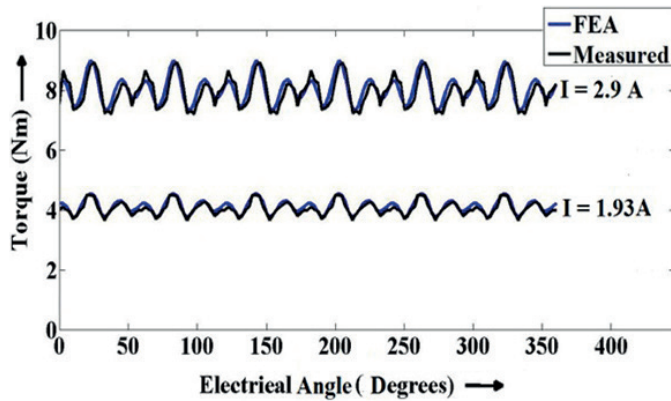


Fig. 7. Experimental result and FEA result of instantaneous torque

The instantaneous torque waveform obtained from FEA and the torque sensor for the PMASR motor under two different load conditions at rated speed is shown in Fig. 7.

The average torque obtained from FEA, analytical calculation and experimental results are tabulated in Table 1 for different load conditions at rated speed. Also, the average torque obtained is in accordance with the dimensions of the motor under rated conditions.

Table 1

Comparison between FEA, analytical and experimental results

Performance parameter	FEA results	Experimental result	Analytical method
Average Torque (T_{av}) ($I = 2.9A$)	8.02 Nm	7.95 Nm	8.13 Nm
Average Torque (T_{av}) ($I = 1.93A$)	4 Nm	3.86 Nm	4.16 Nm

The analytical formula which is used in the determination of average torque of the PMASR motor is given by:

$$T_{av} = \frac{3}{2} \frac{p}{2} [(L_d - L_q) I_d I_q + \lambda_m I_q] \quad (1)$$

where:

L_d, L_q – d axis and q axis inductances

I_d, I_q – d axis and q axis currents

λ_m – permanent magnet flux linkage

The torque ripple percentage obtained from FEA and the experimental method is tabulated in Table 2 for different load conditions at rated speed.

Table 2

Comparison between FEA and experimental results

Performance parameter	FEA results	Experimental result
Torque ripple percentage ($T_{ripple\%}$) ($I = 2.9A$)	20.46%	21.79%
Torque ripple percentage ($T_{ripple\%}$) ($I = 1.93A$)	19.40%	20.6%

The torque ripple percentage is determined using the following:

$$T_{ripple\%} = \frac{T_{max} - T_{min}}{Average\ torque} \times 100. \quad (2)$$

From Fig. 7, Table 1 and Table 2, the closeness of the experimental and analytical results to the results of FEA validates the use of an FEA model in the sensitivity analysis and optimization routine.

3. Sensitivity analysis

This section details the necessity of sensitivity analysis of geometrical parameters of the PMASR motor prior to optimization. The analysis needs to be performed in order to identify the significant geometrical parameters influencing the performance measures. Also, the nature of variation of the sensitivity index for different geometrical parameters when the choice of objectives is changed is highlighted. Sensitivity analysis is carried out by means of two methods, namely h-indexing and level sensitivity method. The h-indexing and level sensitivity methods are statistical methods, involving identification and prioritization of geometrical parameters as strongly sensitive and mildly sensitive for the optimization procedure.

The bounds of the design variables for performance analysis using FEA, subsequently assessed by sensitivity analysis, are illustrated in Table 3. The limits of variation of the parameters are defined by the manufacturing constraints and the possibility of no intersection between any of the flux barriers.

Table 3

Bounds defining the design variables

Parameter	Design bounds
Magnet height, h_1	3–6 mm
Magnet height, h_2	3–6 mm
Magnet height, h_3	3–6 mm
Magnet width, w_1	3–8 mm
Magnet width, w_2	4–12 mm
Magnet width, w_3	5–20 mm
Angular position at air gap, δ_1	10.6–16°
Angular position at air gap, δ_2	24–29°
Angular position at air gap, δ_3	36.5–41°
Flux barrier angle, θ_1	0–6.5°
Flux barrier angle, θ_2	0–6.5°
Flux barrier angle, θ_3	0–6.5°
Air gap, g	0.3–0.6 mm

3.1. H-indexing technique. In this methodology [9], an order of a precedence (sensitivity) index is designated to all the design variables being considered. The h-index is a quantitative metric

based on the ratio of variances that attempts to measure the individual impact of each geometrical parameter on the three optimization objectives – that of average torque, torque ripple percentage and total loss. For each geometric parameter (x_i), the corresponding sensitivity index $H_y(x_i)$ is defined as:

$$H_y(x_i) = \frac{Var(y|x_i)}{Var(y)} \quad (3)$$

where y is the optimization objective (average or torque ripple percentage or total loss), $Var(y|x_i)$ is the conditional variance of y for a given x_i , and $Var(y)$ is the variance of y over the entire data set.

The motor parameters are prioritized into two levels using the sensitivity indices computed from this technique. Sensitivity analysis is performed for two cases, i.e.

1. with average torque (T_{av}) and torque ripple percentage ($T_{ripple}\%$) as objectives.
2. with torque ripple percentage ($T_{ripple}\%$) and total loss (P_{loss}) as objectives.

The two cases are considered in order to portray the variation of the sensitivity index for different geometrical parameters when the choice of objectives is changed, justifying the role of sensitivity analysis prior to optimization. Predefined scripting existing in the FEA software package is utilized to determine the total loss of the motor.

The sensitivity function $G(x_i)$ is then calculated from the indices for:

Case 1

$$G(x_i) = \lambda_1 |H_{av}(x_i)| + \lambda_2 |H_{ripple}(x_i)| \quad (4)$$

Case 2

$$G(x_i) = \lambda_1 |H_{ripple}(x_i)| + \lambda_2 |H_{loss}(x_i)| \quad (5)$$

where

$$\lambda_1 + \lambda_2 = 1, \quad (6)$$

and $|H_{av}(x_i)|$, $|H_{ripple}(x_i)|$ and $|H_{loss}(x_i)|$ are the absolute values of the sensitivity indices of T_{av} , $T_{ripple}\%$ and P_{loss} , respectively. λ_1 and λ_2 are the weighted coefficients of T_{av} and $T_{ripple}\%$ which satisfy (6) for case 1 and λ_1 and λ_2 are the weighted coefficients of $T_{ripple}\%$ and P_{loss} which satisfy (6) for case 2.

λ_1 and λ_2 are chosen as 0.5 in both cases, as both the optimization outcomes, i.e. minimization of torque ripple percentage and maximization of average torque in case 1 and minimization of torque ripple percentage and minimization of total loss in case 2, are of equal significance. In multi-level optimization, the design parameters are then stratified into two levels, based on the threshold value (δ), as:

- strongly sensitive (Level 1) \Rightarrow consisting of parameters with $G(x_i) > \delta$,
- mildly sensitive (Level 2) \Rightarrow consisting of parameters with $G(x_i) \leq \delta$,

where δ – average sensitivity value.

The h-index values obtained for the PMASR motor using (3) for the cases defined in (4) and (5) are tabulated in Table 4 and Table 5, respectively.

Table 4

Sensitivity analysis using H-indices with average torque and torque ripple percentage as objectives

Design variables	$H_{av}(x_i)$	$H_{ripple}(x_i)$	$G(x_i)$
h_1	-0.0293	-0.2153	0.1223
h_2	0.023	0.0274	0.0252
h_3	0.0085	0.0112	0.00985
w_1	0.0200	-0.032	0.026025
w_2	-0.0071	-0.0251	0.0161
w_3	0.0130	-0.0025	0.007785
δ_1	0.8647	-0.7129	0.7888
δ_2	-0.9828	-0.4414	0.7121
δ_3	0.3677	0.0848	0.22625
θ_1	-0.7261	-0.0314	0.37875
θ_2	-0.4716	-0.0124	0.242
θ_3	0.2786	-0.0261	0.15235
g	0.1273	0.2126	0.16995
Average sensitivity value (δ)			0.22134

Table 5

Sensitivity analysis using H-indices with torque ripple percentage and total loss as objectives

Design variables	$H_{ripple}(x_i)$	$H_{loss}(x_i)$	$G(x_i)$
h_1	-0.2153	0.1529	0.1841
h_2	0.0274	0.1481	0.08775
h_3	0.0112	0.09	0.0506
w_1	-0.032	0.1233	0.07765
w_2	-0.0251	0.1134	0.06925
w_3	-0.0025	0.1086	0.05555
δ_1	-0.7129	-0.1284	0.42065
δ_2	-0.4414	-0.1349	0.28815
δ_3	0.0848	-0.1481	0.11645
θ_1	-0.0314	0.1159	0.07365
θ_2	-0.0124	0.1364	0.0744
θ_3	-0.0261	0.1181	0.0721
g	0.2126	0.0109	0.11175
Average sensitivity value (δ)			0.12938

From Table 4, it is observed that δ_1 , δ_2 , θ_1 , θ_2 and δ_3 are the strongly sensitive design variables in the order of highest priority. In Table 5, it is observed that δ_1 , δ_2 and h_1 are the strongly sensitive design variables in the order of highest priority. Therefore, it can be concluded that based on the choice

of objectives, the sensitivity index of design variables changes and priority of choice for the optimization routine also varies. This work focuses on torque ripple minimization along with maximization of average torque. Hence, the sensitivity index calculation will focus on average torque and torque ripple percentage in the sections below.

Also, the following observation can be made from the tables defining the sensitivity index. As per the variance in (3), a design variable with a positive index in the sensitivity indices table aids in the design optimization process while a variable with a negative index exhibits a contradictory nature [10]. For instance, in Table 4, it can be inferred that a positive $H_{av}(x_i)$ indicates a rise in T_{av} along with x_i and a positive $H_{ripple}(x_i)$ indicates a fall in $T_{ripple}\%$ when x_i increases, as the fundamental objective is to increase average torque and reduce torque ripple percentage. Although positive and negative indices denote the impact of all geometric parameters on the design objectives, the vital design variables can be uniquely identified by their high value of absolute cumulative sensitivity index for the design objectives.

3.2. Level sensitivity analysis technique. An alternative scheme [10] for calculating sensitive indices of the different geometrical parameters for PMASR motors involves a systematic level sensitivity analysis technique. In this technique, for each design variable (x_i), the corresponding sensitivity index $S(x_i)$ is defined as the ratio of percentage changes in the objective to the percentage change in the value of the design variable, and can be obtained from the following formula:

$$S_y(x_i) = \frac{\text{Percentage changes in } y(x)}{\text{Percentage changes in } x_i} \quad (7)$$

where y is the optimization objective and x_i represents the independent design variables for the PMASR motor.

The comprehensive level sensitivity index $S_{com}(x_i)$ is then computed from the indices that are chosen so as to satisfy (4). $|S_{av}(x_i)|$ and $|S_{ripple}(x_i)|$ are the absolute values of the level sensitivity indices of T_{av} and $T_{ripple}\%$, respectively. In this methodology, λ_1 and λ_2 are chosen as 0.5, as before, and the geometric parameters are divided into two levels, i.e. strongly sensitive variables with comprehensive sensitivity above the threshold and mildly sensitive variables that are below the set threshold value. The level sensitivity index values obtained for the PMASR motor using (7) for the case defined in (4) is presented in Table 6.

From Table 6, it is observed that $\delta_1, \delta_2, \theta_1, \delta_3$ and θ_2 are the strongly sensitive design variables in the order of highest priority. Similar observations were made in Table 4, validating the earlier results obtained using the h-index sensitivity analysis with slight variations. The minor variations in the prioritization of design variables are due to the reasons discussed below.

The sensitivity indices computed using the level sensitivity analysis technique are influenced by the sample demographics [24], and thus require know-how to collect distributed data samples within the defined boundary constraints, free of any bias against individual variables. The H-indexing technique,

Table 6
Sensitivity analysis using level sensitivity analysis for PMASR motor with average torque and torque ripple percentage as objectives

Design variables	$S_{av}(x_i)$	$S_{ripple}(x_i)$	$S_{com}(x_i)$
h_1	-0.0536	-0.1191	0.08635
h_2	0.0165	0.1546	0.08555
h_3	0.0473	0.1134	0.08035
w_1	0.0316	-0.0597	0.04565
w_2	-0.0164	-0.0467	0.0315
w_3	0.0195	-0.0114	0.01545
δ_1	0.7345	-0.7834	0.75895
δ_2	-0.8745	-0.3419	0.6082
δ_3	0.4655	0.0765	0.271
θ_1	-0.5514	-0.0768	0.3141
θ_2	0.4889	-0.0516	0.2702
θ_3	-0.3497	-0.0168	0.18325
g	0.1116	0.1053	0.10845
Average sensitivity value (δ)			0.21992

on the other hand, models the actual sensitivity of the geometric parameters in a comparative manner. Since the design variables are mutually independent and identically distributed with a finite variance, as per the central limit theorem (CLT), the variance of the sample population is approximately equal to the variance of the original population. The h-indexing technique makes use of the fact that the estimated variances can be fine-tuned by increasing the sample size to systematically compute H-indices and are hence more reliable [25]. Therefore, the optimization routine is based on the prioritization of design variables based on the h-indexing technique.

Contour map representation [8] of variations of average torque and torque ripple percentage with respect to the key design parameters, angular positions at air gap, δ_1 and δ_2 (highest h-index and level sensitivity index) of the PMASR motor for a specific range are shown in Fig. 8 and Fig. 9 to provide an insight into the sensitivity of the design variable.

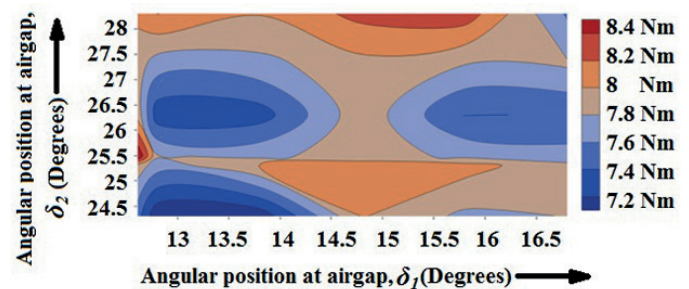


Fig. 8. Influence of change of δ_1 and δ_2 of PMASR motor on average torque

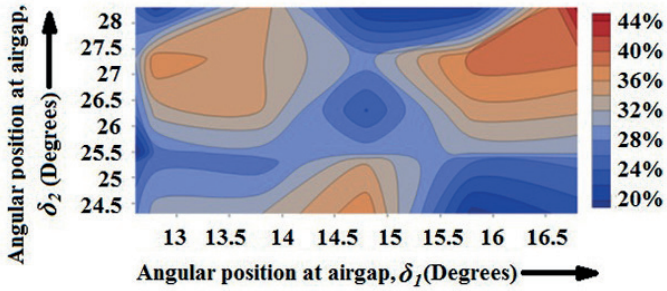


Fig. 9. Influence of change of δ_1 and δ_2 of PMASR motor on torque ripple percentage

4. Design optimization

The design optimization process constitutes a significant aspect of determining significant design solutions of the PMASR motor. This work involves the use of non-dominated sorting genetic algorithm – II (NSGA-II) for performing design optimization. Advantages of the NSGA-II algorithm [13, 14] include better spread of solutions and distinct convergence near the true Pareto-optimum front.

The objective functions are as follows:

- minimization of torque ripple percentage,

$$f_1 = \min(T_{ripple} \%) \quad (8)$$

- maximization of average torque,

$$f_2 = \max(T_{av}). \quad (9)$$

Significant variables based on the h-index used in the multi-level optimization routine [9, 10] are listed in Table 7.

Table 7

Classification of PMASR motor parameters for optimization

Parameter level	Parameters
Level 1 (strongly sensitive variables)	$\delta_1, \delta_2, \theta_1, \theta_2, \delta_3$
Level 2 (mildly sensitive variables)	$g, \theta_3, h_1, w_1, h_2, w_2, h_3, w_3$

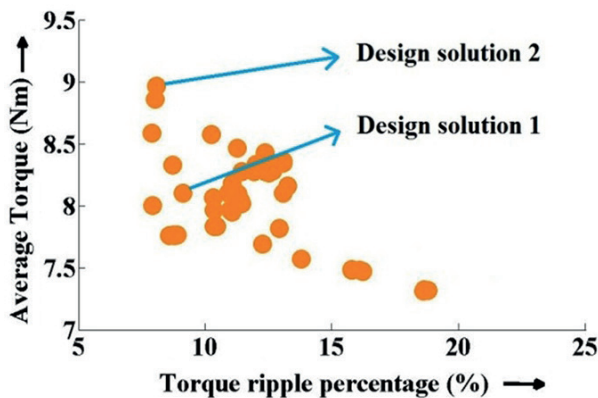


Fig. 10. Pareto distribution of optimized results for PMASR motor

The NSGA-II algorithm has been implemented using MATLAB [26], with the population size = 100, crossover probability = 0.8, mutation probability = 0.33, crossover index = 20; mutation index = 20 and maximum number of iterations = 100. The Pareto distribution of optimization results for the PMASR motor is represented in Fig. 10.

Two significant solutions considering the requirement of torque ripple reduction have been represented in Table 8.

Table 8

Geometrical and performance parameters of selected design solutions of PMASR motor

Parameter	Design solution 1	Design solution 2
Magnet height, h_1	3.5 mm	3 mm
Magnet height, h_2	4.7 mm	4.2 mm
Magnet height, h_3	5.8 mm	5.2 mm
Magnet width, w_1	6.2 mm	6 mm
Magnet width, w_2	10 mm	9 mm
Magnet width, w_3	16 mm	13.3 mm
Angular position at air gap, δ_1	11.5°	12.3°
Angular position at air gap, δ_2	24.9°	25.2°
Angular position at air gap, δ_3	38.1°	38.3°
Flux barrier angle, θ_1	5°	3.3°
Flux barrier angle, θ_2	2.5°	1.8°
Flux barrier angle, θ_3	1.9°	1.2°
Airgap, g	0.52 mm	0.47 mm
Average torque, T_{av}	8.1 Nm	8.96 Nm
Torque ripple percentage, $T_{ripple} \%$	9.13%	8.06%
Total loss, P_{loss}	108.06 W	118.41 W

5. Multiphysics performance analysis

5.1. Thermal analysis. The thermal performance of the PMASR motor prototype and two design solutions obtained as part of the optimization routine are evaluated using the totally enclosed fan cooled (TEFC) type of cooling system, modeled in MotorSolve – the thermal module [22] as the prototype PMASR motor employs the same type of cooling. The ambient temperature is at 25°C. The FEA results obtained are experimentally verified using PT100 temperature sensors, embedded in the prototype motor in the stator core and stator winding, as shown in Fig. 11.

Figure 12 represents the temperature rise curves [18] obtained for different parts of the PMASR motor for a period of 270 minutes of constant load at rated operating conditions. From Fig. 12, it is observed that the FEA and experimental results indicate that temperature rise curves are similar in nature over the period of 270 minutes. A sample reading at 270th



Fig. 11. Experimental setup for estimation of stator core and winding temperature

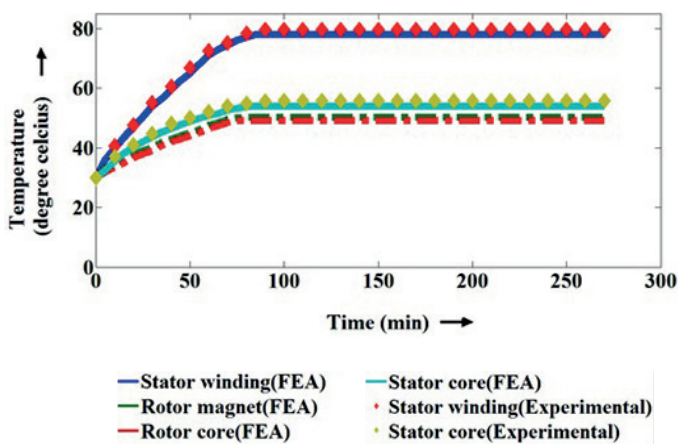


Fig. 12. Temperature rise curves for different parts of PMASR motor

minute using a temperature sensor is represented for comparison with the temperature obtained using FEA in Table 9.

Table 9

FEA vs experimental results of constant rated load operation with fan at time = 270 min

Part	FEA	Experimental
Stator winding	78°C	79.5°C
Stator core	54°C	55.7°C

From Table 9, it can be observed that a good agreement exists between FEA and experimental results, confirming the reliability of the FEA model for prediction of temperature for the rotor core and ferrite magnet located in the flux barriers. The final peak temperatures predicted using FEA for different parts of the PMASR motor after 270 minutes of constant load at rated operating conditions are represented in Fig. 13.

The final peak temperature distribution predicted using FEA for different parts of 1/4th cross section of the PMASR motor after 270 minutes of constant load at rated operating conditions are represented in Fig. 14.

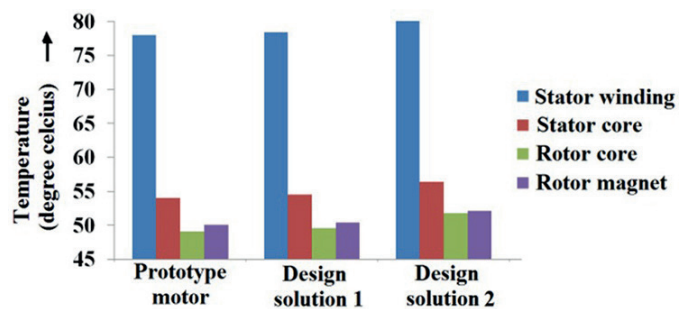


Fig. 13. Comparison of temperatures of different parts of PMASR motor prototype and two design solutions

From Fig. 14, it can be noted that the temperatures are similar for design solution 1 and the prototype motor. The temperatures of the different parts of the motor represented using design solution 2 have increased by 2°C as compared to the other configurations, and the total loss is higher than that of the PMASR motor prototype and design solution 1.

5.2. Stress analysis. The structural performance [18–21] of design solutions is determined using ANSYS [27] FEA software at rated operating conditions. The stresses on flux barriers are due to their anisotropy and the centrifugal forces emerging as results of ferrite magnet housing. Assumptions for the simulation are

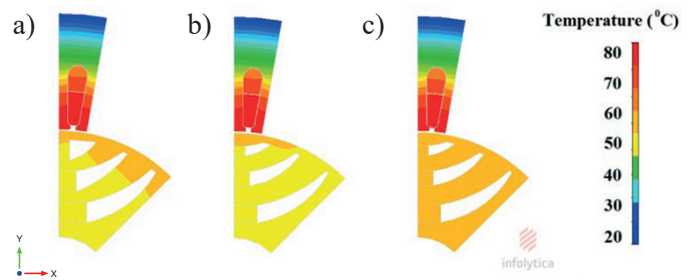


Fig. 14. Comparison of temperature distribution for different parts of 1/8th cross section of PMASR motor (a) prototype (b) design solution 1 and (c) design solution 2

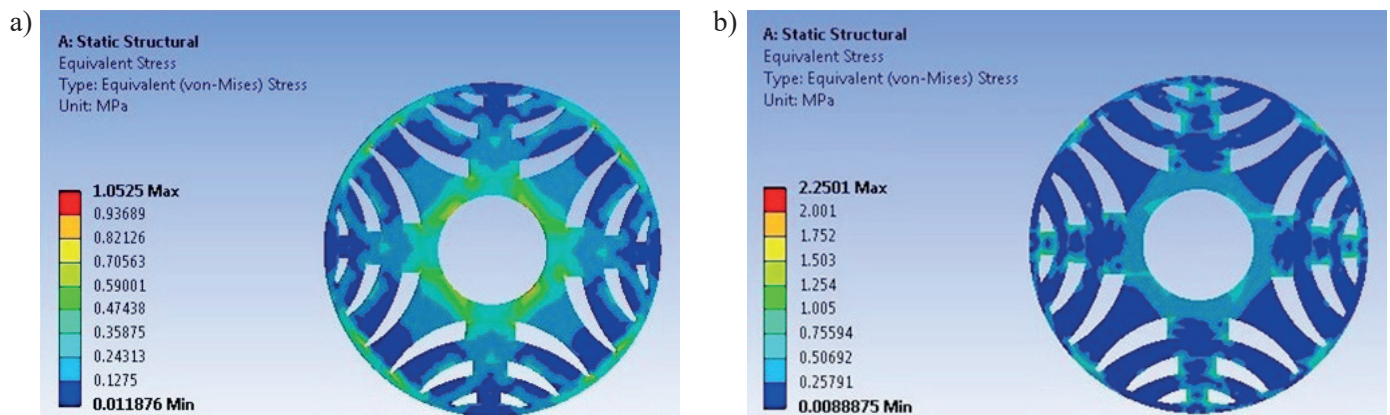


Fig. 15. Von Mises stress distribution of (a) design solution 1 (b) design solution 2 of PMASR motor

made based on [18]. The mass densities of the M1000 type steel used in the rotor core and in the ferrite magnet are 7800 kg/m^3 and 4900 kg/m^3 , respectively. The results of static structural analysis, portraying the von Mises stresses on design solutions 1 and 2 of the PMASR motor, are represented in Fig. 15.

From Fig. 15, it can be seen that the stress induced in design solutions 1 and 2 of the PMASR motor is less than 295 MPa (yield strength of laminations), validating the optimization procedure for obtaining designs with reduced stress owing to reduction in torque ripple.

6. Conclusion

An effective design procedure for determining the influence of geometrical parameter variations on torque ripple and average torque of a PMASR motor is presented clearly in this work. From the sensitivity analysis performed, the strongly sensitive parameters were observed and prioritized for optimization. The design solutions obtained by means of the NSGA-II optimization routine depicted significant minimization of torque ripple and maximization of electromagnetic torque through well-distributed Pareto-optimum planes. The results of this work are verified through multiphysics performance analysis of selected design solutions, indicating stable thermal performance and vibration performance in terms of stress distribution in the rotor.

Acknowledgements. This research was supported and funded by the Department of Science and Technology, the Government of India and the SSN Trust.

REFERENCES

- [1] D.H. Jung, Y. Kwak, J. Lee, and C.S. Jin, "Study on the optimal design of PMA-SynRM loading ratio for achievement of ultra-premium efficiency", *IEEE Trans. Magn.* 53 (6), 1–4 (2017).
- [2] S. Morimoto, S. Ooi, Y. Inoue, and M. Sanada, "Experimental evaluation of a rare-earth-free PMASynRM with ferrite magnets for automotive applications", *IEEE Trans. Ind. Elec.* 61 (10), 5749–5756 (2014).
- [3] H. Cai, B. Guan, and L. Xu, "Low-cost ferrite PM-assisted synchronous reluctance machine for electric vehicles", *IEEE Trans. Ind. Elec.* 61 (10), 5741–5748 (2014).
- [4] K. Wang, Z.Q. Zhu, G. Ombach, M. Koch, S. Zhang, and J. Xu, "Torque ripple reduction of synchronous reluctance machines optimal slot/pole and flux-barrier layer number combinations", *COMPEL – The international journal for computation and mathematics in electrical and electronic engineering* 34 (1), 3–17 (2015).
- [5] M. Gamba, G. Pellegrino, and F. Cupertino, "Optimal number of rotor parameters for the automatic design of synchronous reluctance machines", *Int. Conf. Electrical Machines ICEM* 1334–1340 (2014).
- [6] N. Bianchi, M. Degano, and E. Fornasiero, "Sensitivity analysis of torque ripple reduction of synchronous reluctance and interior PM motors", *IEEE Trans. Ind. Appl.* 51 (1), 187–195 (2015).
- [7] V.S. Nagarajan, M. Balaji, V. Kamaraj, R. Arumugam, N. Ganesh, S. Srivignesh, and M. Suudharshana, "Design optimization of ferrite assisted synchronous reluctance motor using multi-objective differential evolution algorithm", *COMPEL – The international journal for computation and mathematics in electrical and electronic engineering* 36 (1), 219–239 (2017).
- [8] V.S. Nagarajan, V. Kamaraj, M. Balaji, R. Arumugam, N. Ganesh, R. Rahul, and M. Lohit, "Effect of geometrical parameters on optimal design of synchronous reluctance motor", *J. Magn.* 21 (4), 544–553 (2016).
- [9] X. Zhu, Z. Shu, L. Quan, Z. Xiang, and X. Pan, "Multi-objective optimization of an outer-rotor v-shaped permanent magnet flux switching motor based on multi-level design method", *IEEE Trans. Magn.* 52 (10), 1–8 (2016).
- [10] Z. Xiang, X. Zhu, L. Quan, Y. Du, C. Zhang, and D. Fan, "Multilevel design optimization and operation of a brushless double mechanical port flux-switching permanent-magnet motor", *IEEE Trans. Ind. Elec.* 63 (10), 6042–6054 (2016).
- [11] J.K. Sykulski, "Computational electromagnetics for design optimisation: the state of the art and conjectures for the future", *Bull. Pol. Ac.: Tech.* 57 (2), 123–131 (2009).
- [12] P. Kedzierski, A. Morka, G. Slawinski, and T. Niezgodza, "Optimization of two-component armour", *Bull. Pol. Ac.: Tech.* 63 (1), 173–179 (2015).
- [13] K. Deb, A. Pratap, S. Agarwal, and T. Meyarivan, "A fast and elitist multiobjective genetic algorithm: NSGA-II", *IEEE Trans. Evol. Comp.* 6 (2), 182–197 (2002).

[14] Dlugosz and T. Burczynski, “Multiobjective shape optimization of selected coupled problems by means of evolutionary algorithms”, *Bull. Pol. Ac.: Tech.* 60 (2), 215–222 (2012).

[15] S. Berhausen and S. Paszek, “Use of the finite element method for parameter estimation of the circuit model of a high power synchronous generator”, *Bull. Pol. Ac.: Tech.* 63 (3), 575–582 (2015).

[16] Lebkowski, “A way of neodymium-iron-boron magnets regeneration in surface-mounted PMSM used in electric vehicles”, *Bull. Pol. Ac.: Tech.* 65 (5), 751–758 (2017).

[17] Y. Wang, D.M. Ionel, M. Jiang, and S.J. Stretz, “Establishing the relative merits of synchronous reluctance and PM assisted technology through systematic design optimization,” *IEEE Trans. Ind. Appl.* 52 (4), 2971–2978 (2016).

[18] A. Fatemi, N.A. O. Demerdash, T.W. Nehl, and D.M. Ionel, “Large-scale design optimization of PM machines over a target operating cycle”, *IEEE Trans. Ind. Appl.* 52 (5), 3772–3782 (2016).

[19] W. Zhao, F. Xing, X. Wang, T.A. Lipo, and B.I. Kwon, “Design and analysis of a novel PM-assisted synchronous reluctance machine with axially integrated magnets by the finite-element method”, *IEEE Trans. Magn.* 53 (6), 1–4 (2017).

[20] M. Nowak, “Improved aeroelastic design through structural optimization”, *Bull. Pol. Ac.: Tech.* 60 (2), 237–240 (2012).

[21] W. Ostapski, A. Arominski, and S. Dowkontt, “The vibration of prototype aircraft propeller speed reduction unit – test bench and FEM numerical simulation study”, *Bull. Pol. Ac.: Tech.* 62 (4), 861–873 (2014).

[22] MagNet and MotorSolve, Infolytica, <http://www.infolytica.com/>.

[23] G. Extremiana, G. Abad, J. Arza, J. Chivite-Zabalza, and I. Torre, “Rotor flux oriented control of induction machine based drives with compensation for the variation of all machine parameters”, *Bull. Pol. Ac.: Tech.* 61 (2), 309–324 (2013).

[24] P. Brown, “Measure theory and the central limit theorem”, *VIGRE REU* (2011).

[25] Z.R. Smith and C.S. Wells, “Central limit theorem and sample size”, *Annual meeting of the Northeastern Educational Research Association NERA* (2006).

[26] MATLAB, MathWorks, <https://www.mathworks.com/products/matlab.html>.

[27] ANSYS Multiphysics, www.ansys.com/en-in/products/platform/multiphysics-simulation.

7. Appendix

Table A1
Parameters of prototype PMASR motor

Parameter	Value
Rated power	1.2 kW
Rated speed	1500 rpm
Rated torque	8 Nm
Air gap, g	0.45 mm
Radius of rotor	45.6 mm
Inner radius of stator	46.05 mm
Outer radius of stator	79.5 mm
Stack length	64 mm
Shaft radius	15 mm
Magnet height, h_1	6 mm
Magnet height, h_2	6 mm
Magnet height, h_3	6 mm
Magnet width, w_1	6 mm
Magnet width, w_2	10 mm
Magnet width, w_3	16 mm
Angular position at air gap, δ_1	14.8°
Angular position at air gap, δ_2	26.3°
Angular position at air gap, δ_3	38.8°
Flux barrier angle, θ_1	0°
Flux barrier angle, θ_2	1.9°
Flux barrier angle, θ_3	2.1°
Iron rib thickness, t	2 mm
Type of electrical steel	M1000
Type of permanent magnet	Ferrite-Y30
Remanence	0.37T
d – axis inductance, L_d	0.441 H
q – axis inductance, L_q	0.102 H
Total loss	110.6 W